

# Targeting oxidative phosphorylation to increase the efficacy of immune-combination therapy in renal cell carcinoma

Jihua Tian,<sup>1,2</sup> Jing Luo,<sup>3</sup> Xing Zeng,<sup>1</sup> Chunjin Ke,<sup>1</sup> Yanan Wang,<sup>1</sup> Zhenghao Liu,<sup>1</sup> Le Li,<sup>1</sup> Yangjun Zhang,<sup>1</sup> Zhiquan Hu,<sup>1</sup> Chunguang Yang <sup>1</sup>

**To cite:** Tian J, Luo J, Zeng X, et al. Targeting oxidative phosphorylation to increase the efficacy of immune-combination therapy in renal cell carcinoma. *Journal for ImmunoTherapy of Cancer* 2024;**12**:e008226. doi:10.1136/jitc-2023-008226

► Additional supplemental material is published online only. To view, please visit the journal online (<https://doi.org/10.1136/jitc-2023-008226>).

JT and JL contributed equally.  
Accepted 22 January 2024



© Author(s) (or their employer(s)) 2024. Re-use permitted under CC BY-NC. No commercial re-use. See rights and permissions. Published by BMJ.

<sup>1</sup>Department of Urology, Tongji Hospital Affiliated Tongji Medical College of Huazhong University of Science and Technology (HUST), Wuhan, China

<sup>2</sup>Department of Urology, Zhujiang Hospital, Southern Medical University, Guangzhou, Guangdong, China

<sup>3</sup>Institute of Reproductive Health, Center for Reproductive Medicine, Tongji Medical College, Huazhong University of Science and Technology, Wuhan, China

## Correspondence to

Dr Chunguang Yang;  
cgyang-hust@hotmail.com

Zhiquan Hu;  
huzhiquan2000@163.com

## ABSTRACT

**Background** Immune checkpoint inhibitors (ICIs) are the standard of care for metastatic renal cell carcinoma (RCC); however, most patients develop de novo or acquired resistance to ICIs. Oxidative phosphorylation (OXPHOS) has been rarely explored as a potential target for correcting ICI resistance.

**Methods** We systematically analyzed RNA sequencing and clinical data from CheckMate, JAVELIN Renal 101, and NCT01358721 clinical trials, and clinicopathological data of 25 patients from Tongji Hospital to investigate the relationship between OXPPOS and ICI resistance. The *Ndufb8*-knockdown Renca cell line was derived to determine the effect of OXPPOS on RCC immunotherapy in vivo.

**Results** An analysis of the CheckMate series data revealed that high OXPPOS levels are risk factors for ICI in patients with RCC, but are affected by the von Hippel-Lindau protein (VHL) and hypoxia-inducible factor-1 $\alpha$  status. This result is consistent with correlation between clinicopathological characteristics and prognostic observations at our institute. Knockdown of the mitochondrial complex I subunit *Ndufb8* of the Renca cell line had no effect on cell growth and migration in vitro, but slowed down cell growth in vivo. Among anti-programmed death ligand 1 (PD-L1)-treated BALB/c mice, sh*Ndufb8* Renca tumors grew slower than shControl Renca tumors and the corresponding mice survived longer. Flow cytometry revealed that CD8<sup>+</sup> T cells in sh*Ndufb8* Renca tumors, which were exposed to a lower degree of hypoxia and expressed less programmed death-1 (PD-1) and T-cell immunoglobulin domain and mucin domain 3 (TIM-3), secreted more interferon- $\gamma$  after stimulation. Immunofluorescence demonstrated that the sh*Ndufb8* Renca tumors had a higher proportion of CD8<sup>+</sup> T cells and the proportion of these cells was lower in the hypoxic area.

**Conclusions** OXPPOS is a reliable predictor of immunotherapy response in RCC and is more pronounced in metastatic lesions. RCC cells generate a hypoxic tumor microenvironment and inhibit T-cell function through oxidative metabolism, thereby leading to immunotherapy resistance.

## WHAT IS ALREADY KNOWN ON THIS TOPIC

⇒ Oxidative phosphorylation (OXPHOS) has shown inhibitory effects in immunotherapy of melanoma, but its role in immune checkpoint inhibitor treatment of renal cell carcinoma is unknown.

## WHAT THIS STUDY ADDS

⇒ This study found that OXPPOS is a risk factor for resistance to immune checkpoint inhibitors treatment in renal cell carcinoma by analyzing data from CheckMate, NCT01358721, Javelin Renal 101 and Tongji Hospital. And it was verified through in vitro and in vivo experiments.

## HOW THIS STUDY MIGHT AFFECT RESEARCH, PRACTICE OR POLICY

⇒ This study provides a theoretical basis for the use of oxidative phosphorylation inhibitors to improve resistance to immune checkpoint inhibitors in renal cell carcinoma.

## INTRODUCTION

Immune checkpoint inhibitors (ICIs) have changed the treatment scenario of advanced or metastatic renal cell carcinoma (a/mRCC). Compared with tyrosine kinase inhibitors (TKIs) alone, ICIs alone or ICIs combined with TKIs significantly improved the progression-free survival (PFS) and overall survival (OS) of a/mRCC. The ICI arm achieved a complete remission of approximately 10%.<sup>1–4</sup> ICIs or ICIs combined with TKI have replaced TKIs as the current first-line treatment for a/mRCC, but only approximately 38%–55.7% of patients respond to ICIs.<sup>1–3,5</sup> Identifying and correcting unfavorable factors may help screen out ICI-resistant patients and allow them to benefit from ICI treatment.

The tumor microenvironment (TME) is possibly an ideal entry point. TME plays a crucial role in ICI resistance by affecting immune cells.<sup>6,7</sup> Compared with normal



tissues, the TME has evident characteristics of hypoxia, which can significantly affect the function of immune cells, especially T cells,<sup>8,9</sup> whereas tumor cells are less affected by hypoxia because of their preference for glycolysis, and heterogeneity occurs due to different degrees of hypoxia in their regions.<sup>10</sup>

Oxidative phosphorylation (OXPHOS) is among the main ways of eukaryotic synthesis of adenosine triphosphate (ATP). Although tumor cells prefer glycolysis in an aerobic environment,<sup>11–13</sup> they continue to retain the function of mitochondrial OXPHOS, and some products of OXPHOS such as ROS, ATP, and aspartic acid are crucial for tumor cell survival and development.<sup>14–21</sup> Tumor cells can consume oxygen through OXPHOS to promote the formation of a hypoxic TME and T-cell exhaustion.<sup>22</sup>

By analyzing the data of published randomized controlled trials, we here found that OXPHOS is a critical factor for immunotherapy resistance in RCC, which is more pronounced in metastatic lesions, consistent with the clinicopathological and prognostic characteristics in our institute. Moreover, the role of OXPHOS was verified by in vivo and in vitro experiments.

## METHODS

### Cohorts and patients

Thirty-three a/mRCC cases treated with ICIs were from the discovery and validation cohort of *Diana Miao et al.*<sup>23</sup> All of these cases were resistant to TKI and were receiving nivolumab therapy.

The CheckMate series mainly included cases of TKI-treated and TKI-resistant a/mRCC with clear cell components (995 TKI-treated and TKI-resistant cases, 10 TKI-naïve cases). Among them, 311 cases (which included TKI-treated and TKI-resistant cases) underwent RNA sequencing. Of the 311 cases, 130 cases received everolimus monotherapy and 181 cases received nivolumab monotherapy.<sup>24</sup>

The JAVELIN Renal 101 study included 726 cases of TKI-naïve a/mRCC with clear cell components who underwent RNA sequencing, of which 372 cases received sunitinib monotherapy and 354 cases received avelumab plus axitinib.<sup>25</sup>

The NCT01358721 study enrolled 72 patients with a/mRCC who underwent RNA sequencing and received nivolumab monotherapy. Among them, 59 patients underwent RNA sequencing before receiving nivolumab treatment. Among the 59 patients, 41 were TKI-treated and TKI-resistant cases, and 18 were TKI-naïve cases. Among the four arms of the study, arms A, B, and C included TKI-treated and TKI-resistant cases, and arm D included TKI-naïve cases. Arms A, B, C, and D received nivolumab at 0.3 mg/kg every 3 weeks, 2 mg/kg every 3 weeks, 10 mg/kg every 3 weeks, and 10 mg/kg every 3 weeks, respectively. Post-treatment RNA sequencing was performed in 55 of the

72 cases on day 8 of the second cycle after receiving nivolumab.<sup>26</sup>

The clinicopathological data of 25 patients in Tongji Hospital were collected and analyzed retrospectively. The evaluation was based on Response Evaluation Criteria In Solid Tumors version 1.1 (RECIST v1.1).<sup>27</sup>

### Statistical analysis

All data analyses were performed using R V.4.2.1 (Institute for Statistics and Mathematics, Vienna, Austria; www.r-project.org). Gene differential expression analysis was performed using the limma package. Differentially expressed genes were defined as a fold change of >2 or <-2 and a p value of <0.05. The OXPHOS score and TKI-Resist scores were analyzed using the SSGSEA package. The t-test was conducted for normally distributed continuous variables, and non-parametric tests were conducted for non-normally distributed continuous variables. Kaplan-Meier analysis was performed to evaluate survival data.

### Cell line, mice, and agents

Renca and 293T were obtained from American Type Culture Collection (ATCC), *Ndufb8*-knockdown Renca cell line was generated through lentiviral transfection. The cells were cultured in Dulbecco's Modified Eagle Medium (DMEM) containing 10% fetal bovine serum at 37°C in a humidified incubator with 5% CO<sub>2</sub>.

In vivo experiments were approved by the Animal Care and Use Committee of Tongji Hospital (TJH-201910012). Female BALB/c mice (age: 4–6 weeks) were purchased from Beijing Vital River Experimental Animal Technology (Beijing, China) and raised under optimal light, temperature, and humidity conditions, with free access to food and water. For the subcutaneous tumor model, 1×10<sup>6</sup> Renca cells were resuspended in 200 µL of phosphate-buffered saline and inoculated subcutaneously into the right flank of the mice. Five days after tumor cell inoculation, InVivoMab antimouse programmed death ligand 1 (PD-L1) (Bio X Cell, #BE0101) was injected intraperitoneally at 200 µg/mouse, and then, this was repeated every 3 days. Each mouse received the treatment four times. The tumor size was measured using a caliper every 3 days, and the tumor volume (mm<sup>3</sup>) was calculated as follows:  $V = \frac{a \times b^2}{2}$  (where V is the volume, and a and b are the longest and shortest diameters of the tumor, respectively). A tumor volume of 2,000 mm<sup>3</sup> in the mice or the death of the mice was considered as the survival endpoint. In each of the sh*Ndufb8* and shControl groups, mice prepared for immunofluorescence and flow cytometry were reared separately, and the tumors were harvested when their diameters became 5–6 mm.

### Retroviral RNA interference

The interference sequences of sh*Ndufb8* 1 and sh*Ndufb8* 2 were GGATGTCATGTGTAACATCT and GGGA

CCTAGACATGTACATCA, respectively. The interference sequence of shControl was ATGGTAGCGTACACTT ATGAT. The aforementioned three shRNAs were packaged and transfected into 293T cells. The resulting virus cells were concentrated and transfected into Renca cells. Screening was performed using puromycin.

### Immunoblot analysis

The cells were lysed using Radio Immunoprecipitation Assay (RIPA) lysis buffer. The lysates were resolved through sodium dodecyl sulfate-polyacrylamide gel electrophoresis on 12% Bio-Rad gels and transferred to polyvinylidene fluoride membranes. The membranes were blocked in tris-buffered saline with Tween-20 (TBST) containing 3% non-fat dry milk. Then, the membranes were treated with primary antibodies, including containing *Ndufb8* (#67690-1-Ig, 1:5000, Proteintech), HIF-1 $\alpha$  (#A22041, 1:500, Abclonel), beta-2 microglobulin (B2m) (#66207-1-Ig, 1:1000, Proteintech), and  $\beta$ -Actin (#E-AB-48018, 1:2000, Elabscience), diluted in an antibody diluent (#RK05743, Western Antibody Dilution Buffer) overnight at 4°C. Then, the secondary antibody (Abclonel, #AS003) was added to the antibody diluent and incubated at room temperature for 1 hour. Chemiluminescence was observed using a ChemiDoc XRS+System (Bio-Rad). Densitometric analysis was performed on the digitally captured film by using ImageLab software (Bio-Rad).

### Flow cytometry

Tumors were harvested and incubated at 37°C in a DMEM medium containing type IV collagenase (1 mg/mL, Sigma), hyaluronidase (1 mg/mL, Sigma), and DNase I (20 U/mL, Sigma). Enzymatic digestion was allowed to occur for 30 min to generate a single-cell suspension, or mechanical dissociation from the harvested tissue was performed. The red blood cells were lysed in the red blood cell lysis buffer (Sigma). The lymphocytes were then separated through centrifugation with 40% and 80% Percoll and cultured at 37°C for 8 hours after stimulation blocking (Cell Stimulation and Protein Transport Inhibitor Kit, #E-CK-A091). The cells were then stained with the following antimouse antibodies for 30 min: CD8 (Elab Fluor Red 780, #E-AB-F1104S, 1:250, Elabscience), CD45 (Elab Fluor Violet 450, #E-AB-F1136Q, 1:250, Elabscience), IFN- $\gamma$  (APC, #E-AB-F1101E, 1:250, Elabscience), TIM-3 (PE, #E-AB-F1192D, 1:250, Elabscience), programmed death-1 (PD-1) (PerCP/Cyanine5.5, #E-AB-F1131J, 1:250, Elabscience), 11.23.22.r Rat FITC-Mab (FITC, #HP6-100Kit, 1:100, Hypoxyprobe). The antibody against intracellular molecules was fixed and ruptured (Intracellular Fixation/Permeabilization Buffer Kit, #E-CK-A109, Elabscience). Data were acquired through multiparameter flow cytometry on a Beckman flow cytometer (Beckman Coulter, Guangzhou, China) and analyzed using FlowJo (Tree Star, Ashland, Oregon, USA) for subsequent studies.

### Histological analysis

For immunohistochemistry (IHC), formalin-fixed, paraffin-embedded tissue sections were deparaffinized. Following antigen retrieval, slides were stained with H&E or corresponding antibodies (anti-MDH2, #A04803-2, 1:100; anti-PD-L1, #BM4816, 1:50; anti-NDUFB8, #A07936-1, 1:100; anti-NDUFS4, #M03608-1, 1:100; HSD17B10, #PB0299, 1:200; Boster, Wuhan, China). The method of staining used was the same as that used in the previous study.<sup>28</sup> For immunofluorescence, pimonidazole HCL (Hypoxyprobe) solution was injected through the tail vein 1 hour before the tumors were harvested and fixed with 4% paraformaldehyde. Then, the tumor tissue was sectioned and stained with antibodies. 4',6-diamidino-2-phenylindole (DAPI) was used to stain the nucleus of the tissue. Anti-hypoxyprobe (11.23.22.r Rat FITC-Mab, #HP6-100Kit, 1:100, Hypoxyprobe) marked the hypoxic area, and anti-Mouse CD8a (CoraLite Plus 647, #CL647-65069, 1:500) labeled CD8+T cells. Fluorescence images were visualized and captured using a confocal laser scanning microscope (Nikon Eclipse TI-SR, DS-U3).

## RESULTS

### OXPHOS predicts the response to ICIs in the CheckMate cohort but not in JAVELIN Renal 101

The RNA sequencing (RNA-seq) (transcripts per million (TPM)) data of response (complete response (CR), partial response (PR)) and non-response (progressive disease (PD), stable disease (SD)) cases from Diana Miao's study were analyzed for differential gene expression. The upregulated genes of non-response cases were significantly enriched in the OXPHOS pathway ( $p < 0.001$ , figure 1A, B). The OXPHOS score of each tumor sample in the CheckMate series was assessed using the SSGSEA algorithm. High OXPHOS levels were risk factors for PFS ( $p = 0.039$ ) and OS ( $p = 0.038$ ) in the nivolumab arm (figure 1C, E) but not in the everolimus arm (PFS,  $p = 0.88$ ; OS,  $p = 0.59$ , figure 1D, F).

Subsequently, we validated these results against those of the JAVELIN Renal 101 cohort and found that OXPHOS levels could not predict patient prognosis in this cohort (avelumab+axitinib arm,  $p = 0.39$ ; sunitinib arm,  $p = 0.14$ , online supplemental figure S1A, B).

As the prognosis of patients with RCC with different glucose metabolism characteristics may be different, the prognosis of high OXPHOS and low OXPHOS groups in the The Cancer Genome Atlas-kidney renal clear cell carcinoma (TCGA-KIRC) cohort were compared. We found that the low OXPHOS group had worse OS ( $p = 0.024$ ) and disease-free survival (DFS) ( $p = 0.0047$ , online supplemental figure S1C, D). To this end, we divided all cases in the JAVELIN Renal 101 cohort into high and low OXPHOS groups and observed the difference in survival between the avelumab+axitinib and sunitinib arms in these two

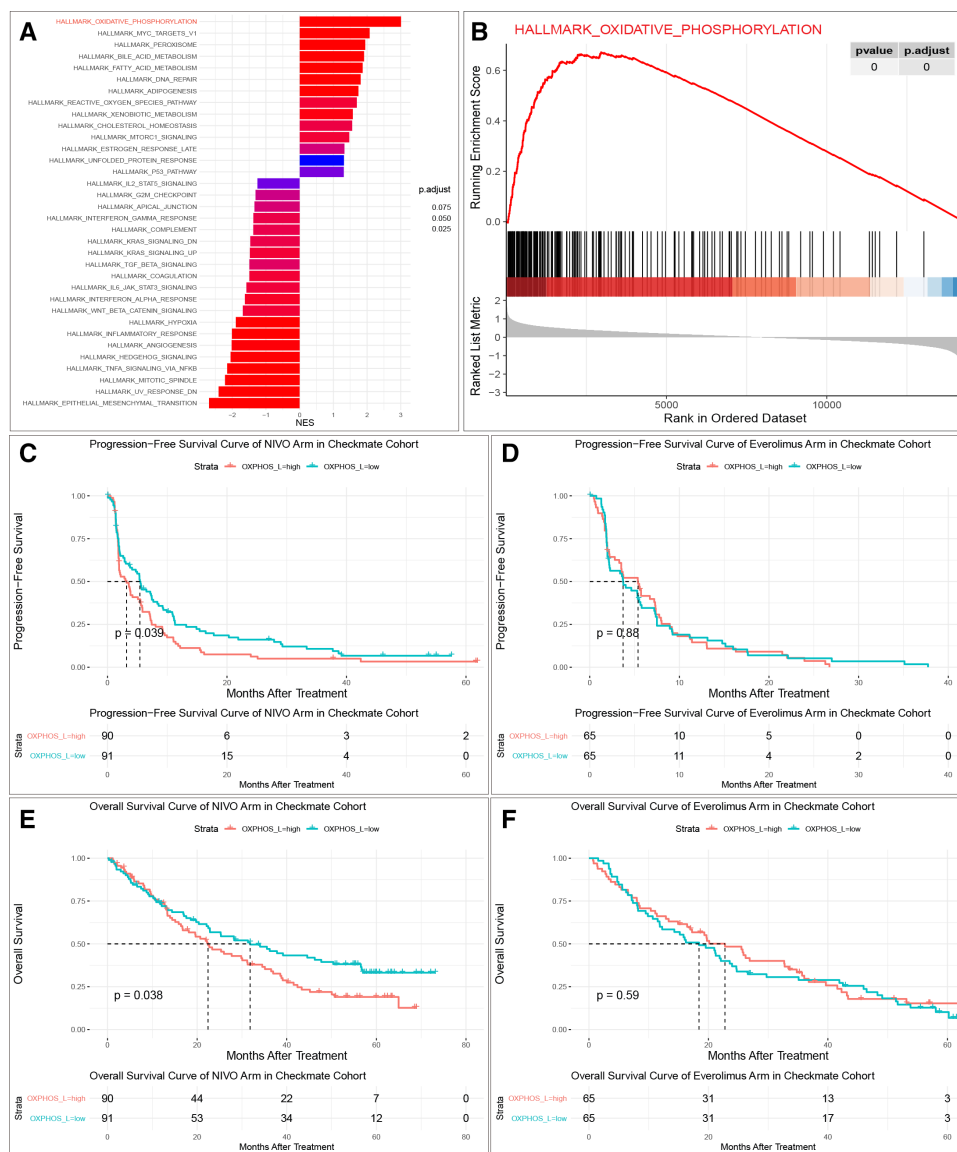


**Figure 1** OXPPOS predicts response and PFS in ICB-treated renal cell carcinoma cases in CheckMate studies. (A) GSEA of differentially expressed genes in PD and SD cases when compared with PR and CR cases indicated that the OXPPOS pathway was significantly upregulated. (B) The OXPPOS pathway enrichment score display ( $p < 0.001$ ). (C) High OXPPOS levels were associated with poorer PFS in the nivolumab arm ( $p = 0.039$ ). (D) OXPPOS were not associated with PFS in the everolimus arm ( $p = 0.088$ ). (E) High OXPPOS were associated with poorer OS in the nivolumab arm ( $p = 0.038$ ). (F) OXPPOS were not associated with OS in the everolimus arm ( $p = 0.59$ ). CR, complete response; GSEA, gene set enrichment analysis; ICB, immune checkpoint blockade; OS, overall survival; OXPPOS, oxidative phosphorylation; PD, progressive disease; PFS, progression-free survival; PR, partial response; SD, stable disease.

groups. Patients in the avelumab+axitinib arms had a better prognosis in both high and low OXPPOS groups (high,  $p = 0.017$ ; low,  $p = 0.0015$ , online supplemental figure S1E, F).

Although the avelumab+axitinib arm exhibited advantages in both groups, the advantage was more significant in the low OXPPOS group. This suggested that high OXPPOS levels had a greater impact on patient prognosis in the avelumab+axitinib arm than in the sunitinib arm in the JAVELIN Renal 101 cohort, but the impact was not sufficiently significant.

Together, these data suggest that OXPPOS predicts the RCC response to ICIs under certain conditions, but these conditions must be elucidated.

#### The ability of OXPPOS to predict ICI resistance correlates with TKI resistance

Although OXPPOS in the JAVELIN Renal 101 cohort tended to hinder ICI response, its effect was not sufficiently significant. To explore why OXPPOS served as a risk factor in the CheckMate cohort, but its impact was not sufficiently significant in the JAVELIN Renal cohort, we analyzed the characteristics of the two cohorts. The

CheckMate cohort was mainly composed of TKI-resistant RCC cases, whereas the JAVELIN Renal cohort consisted mainly of TKI-naïve RCC cases. Therefore, TKI resistance is possibly a major reason for the difference in OXPPOS performance in the two cohorts.

The data from NCT01358721 confirmed this conjecture. This study included 41 TKI-resistant patients and 18 TKI-naïve patients. These patients were divided into four arms, where arms A, B, and C included TKI-resistant patients, whereas arm D included TKI-naïve patients. The baseline gene array data were used to calculate the OXPPOS score of each sample. The OXPPOS score was a risk factor for PFS in the TKI-resistant arms (A, B, C) ( $p=0.045$ , figure 2A), but not in the TKI-naïve arm (D) ( $p=0.077$ , figure 2B).

Because a lower dose of nivolumab was administered to arm A, which resulted in poorer PFS, we analyzed the effect of OXPPOS on PFS in patients separately in arms B and C and found that the effect was more significant in arms B and C ( $p=0.0088$ , figure 2C).

On analyzing the differentially expressed genes between the TKI-resistant arms and the TKI-naïve arm of the NCT01358721 cohort, we obtained the upregulated genes (TRMT5, KCTD1, and GPHN) in the TKI-resistant arms. These genes were then used to assess TKI-resistant characteristics (TKI-Resist signature) (online supplemental figure S2A). For each sample, the TKI-Resist score was calculated in the NCT01358721 cohort. The score of the TKI-resistant arms was significantly higher than that of the TKI-naïve arm ( $p<0.001$ , online supplemental figure S2B). The TKI-Resist score of the JAVELIN Renal cohort samples was also calculated. The predictive ability of OXPPOS was evaluated in the high and low TKI-Resist score groups. In the high TKI-Resist score and high OXPPOS group, no statistically significant difference in PFS was observed between patients who received avelumab+axitinib and those who received sunitinib ( $p=0.20$ , online supplemental figure S2C). In the high TKI-Resist score and low OXPPOS group, patients who received avelumab+axitinib had significantly better PFS than those who received sunitinib ( $p=0.0078$ , online supplemental figure S2D). In the low TKI-Resist score and high OXPPOS group, the avelumab+axitinib achieved a more favorable PFS than sunitinib ( $p=0.028$ , online supplemental figure S2E). In the low TKI-Resist score and low OXPPOS group, patients who received avelumab+axitinib also tended to have better PFS ( $p=0.052$ , online supplemental figure S2F). Taken together, these data indicate that the TKI resistance status of patients affects the ability of OXPPOS to predict the RCC response to ICIs.

### The ability of OXPPOS to predict ICI resistance correlates with histology

All patients included in the JAVELIN Renal 101 cohort had RCC with clear cell components and may have included patients with RCC of other pathological types as the main components. Therefore, we assumed that further classification of the included cases can increase the accuracy of the prediction model.

To obtain the specific RCC classification of the JAVELIN Renal 101 cohort, we analyzed the differentially expressed genes in the three RCC cohorts of TCGA. The results revealed the top four highly expressed genes of the four types (clear cell renal cell carcinoma (ccRCC), papillary renal cell carcinoma (pRCC) type I and II, and chromophobe renal cell carcinoma (chRCC)) as characteristic genes. The characteristic genes of ccRCC, pRCC type I, pRCC type II, and chRCC were CA9, ANGPTL4, NDUFA4L2, and GSTA1; SLC34A2, SOSTDC1, RBP4, and TACSTD2; AKR1B10, NQO1, TSKU, and NEFL; RHCG, FOXI1, KLK1, and PVALB, respectively. Unsupervised clustering was performed in the RCC cohorts of TCGA for verification. The clustering effect among ccRCC, pRCC, and chRCC was favorable, exhibiting the reliability of 16 characteristic genes (online supplemental figure S3A).

We then used the 16 genes obtained for clustering of RCC in the JAVELIN Renal 101 cohort, and this resulted in four clusters (online supplemental figure 3B). The heatmap showed that clusters 1, 2, 3, and 4 highly expressed the characteristic genes of ccRCC, pRCC II, pRCC I, and chRCC, respectively (online supplemental figure S3B). Principal component analysis revealed a high degree of discrimination among the clusters (online supplemental figure S3C). The Von Hippel-Lindau protein (VHL) mutation frequency of cluster 1 was significantly higher than that of other clusters (online supplemental figure S3D). The TKI-Resist score was also significantly higher in cluster 1 than in the other clusters (online supplemental figure S3E). This result is consistent with the results of previous studies that the proportion of VHL mutation was higher in clear cell carcinoma than in the other types of RCC, and patients with RCC having VHL mutations were more sensitive to angiogenesis inhibitors. According to the results of the survival analysis of each cluster, the prognoses of cluster 2 in the sunitinib arm ( $p<0.001$ ) and in the avelumab+axitinib arm ( $p=0.039$ ) were worse than those of cluster 1 (online supplemental figure S3F, G), which is consistent with the results of previous studies, wherein the prognosis of papillary type II RCC was worse than that of clear cell RCC.

Next, we analyzed the effect of OXPPOS on each cluster. In cluster 1, the PFS of the avelumab+axitinib arm was better than that of the sunitinib arm in the low OXPPOS group ( $p=0.015$ , online supplemental figure 4B). However, the difference between the two arms was significant in the high OXPPOS group ( $p=0.043$ , online supplemental figure 4A). In clusters 2, 3, and 4, differences were only significant in the low OXPPOS group ( $p=0.016$ , online supplemental figure 4D), whereas no significant difference was observed in the high OXPPOS group ( $p=0.21$ , online supplemental figure 4C).

The TKI-Resist score was significantly lower in cluster 1 than in the other clusters, whereas the proportion of VHL mutations was significantly higher in cluster 1 than in the other clusters. In terms of prediction of the response to ICIs, OXPPOS in cluster 1 was not as stable as that in the

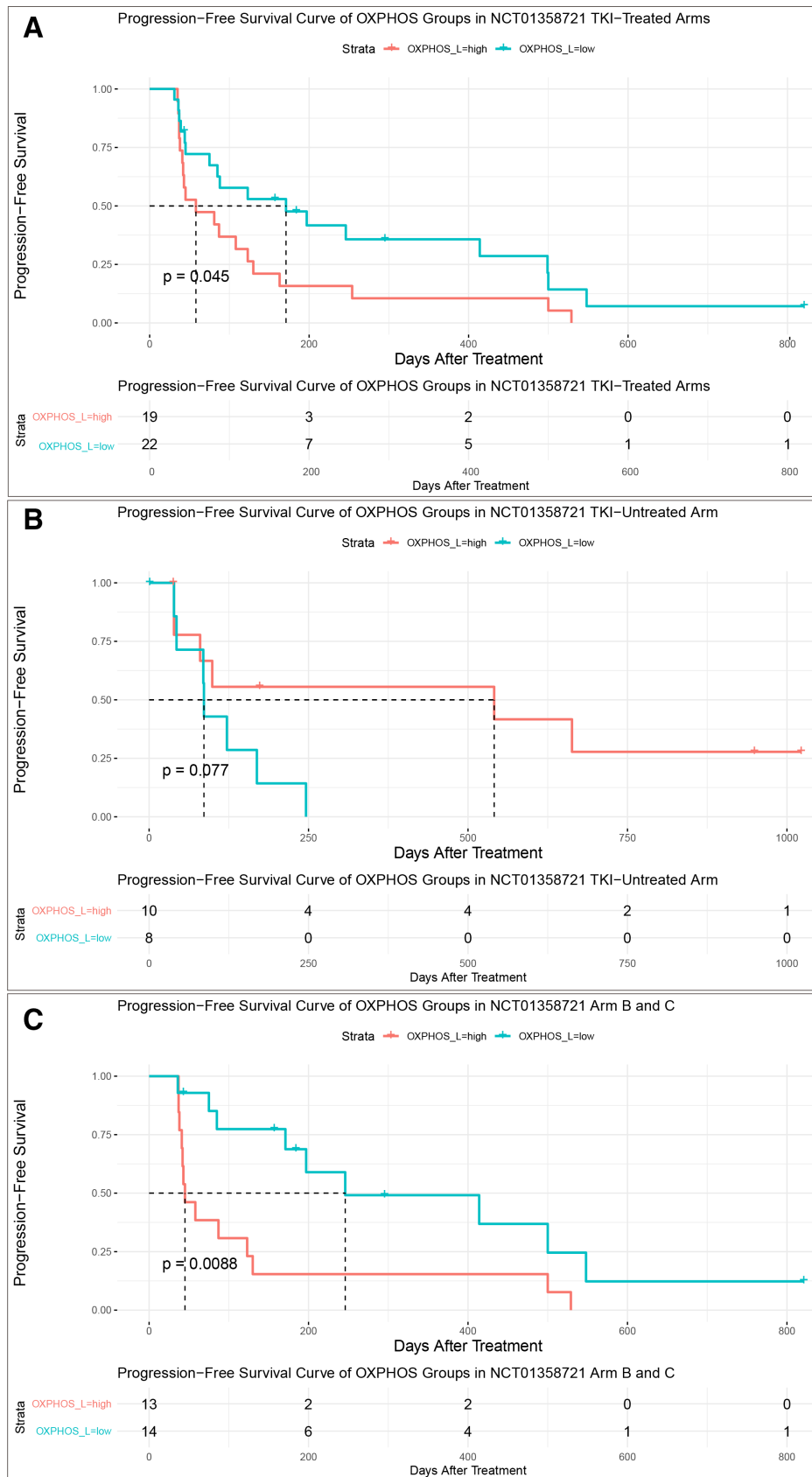


**Figure 2** The OXPPOS predicts PFS in each group of NCT01358721. (A) Higher OXPPOS in the TKI-resistant arms (arms A, B, and C) were associated with poorer PFS ( $p=0.045$ ). (B) OXPPOS were not associated with PFS in the TKI-naïve arm (arm D) ( $p=0.077$ ). (C) Higher OXPPOS in the TKI-resistant arms (arms B and C) were associated with poorer PFS ( $p=0.0088$ ). OXPPOS, oxidative phosphorylation; PFS, progression-free survival; TKI, tyrosine kinase inhibitors.

other clusters. In terms of the VHL status, the VHL mutation ratio of the CheckMate series was lower than that of the JAVELIN Renal 101 cohort (45.98% vs 55.4%, online supplemental figure S5A). The TKI-Resist score was also significantly lower in the VHL mutation cases than in the VHL wild-type cases ( $p=0.0021$ , online supplemental figure S5B). Therefore, the VHL gene status may have an interfering role in the ability of OXPPOS to predict the response to ICIs.

### VHL and hypoxia-inducible factor-1 $\alpha$ status can interfere with OXPPOS to predict ICI resistance

The conjecture is based on the molecular basis. OXPPOS is the main life activity of oxygen consumption that occurs in mitochondria. OXPPOS is negatively regulated by many molecules. The genes that encode these molecules include NDUFA4L2, PDK1, etc<sup>29,30</sup> and are regulated by hypoxia-inducible factor-1 (HIF-1). HIF-1 is a key transcription factor for cells in response to hypoxia. It is a heterodimer composed of a  $\beta$  subunit and an  $\alpha$  subunit and is regulated by the oxygen concentration. Under normoxic conditions, HIF-1 $\alpha$  subunit levels are regulated through ubiquitin-dependent proteasomal degradation. In this  $\alpha$  subunit, the conserved proline residues are hydroxylated by O<sub>2</sub>-dependent prolyl hydroxylases (PHD), while the modified residues are ubiquitinated by the E3 ubiquitin ligase complex containing the VHL protein (pVHL). The subunit is then degraded by the proteasome. However, under hypoxic conditions, the HIF-1 $\alpha$  subunit is stabilized because PHD activity is inhibited, and the subunit then accumulates in the nucleus.<sup>31</sup> The hypoxia response element binds to HIF-1 $\beta$  and regulates the transcription of numerous genes in different pathways, such as angiogenesis, erythropoiesis, apoptosis and survival, cell proliferation, and metabolic reprogramming to allow cells to adapt cells.<sup>32–34</sup> However, the HIF-1 $\alpha$  protein level is not always consistent with the hypoxia level. In the absence of VHL protein expression, the proteasome cannot degrade HIF-1 $\alpha$ , which results in increased HIF-1 activity.

ccRCC accounts for approximately 80% of RCC, and approximately 85% of ccRCC lack VHL activity because of somatic/germline mutation or epigenetic alteration. VHL inactivation can be inhibited at the post-transcriptional level through HIF-1 $\alpha$  stabilization. Therefore, the OXPPOS score calculated using the RNA-seq data in ccRCC cannot reflect the true oxidative metabolism level of the samples.

We therefore grouped the cohorts according to the VHL status of the samples and then verified the relationship between OXPPOS and survival in each group. In the VHL mutant NCT01358721 cohort, no significant difference in PFS was observed between the high and low OXPPOS groups ( $p=0.78$ , online supplemental figure S6A). However, in the VHL wild-type NCT01358721 cohort, the PFS of the high OXPPOS group was significantly worse than that of the low OXPPOS group ( $p=0.02$ , online supplemental figure S6B). In the VHL mutated and TKI-naïve NCT01358721 cohort, no significant difference in PFS was observed between the high and low OXPPOS

groups ( $p=0.85$ , online supplemental figure S6B). In the VHL wild-type and TKI-naïve NCT01358721 cohort, PFS was significantly worse in the high OXPPOS group than in the low OXPPOS group ( $p=0.039$ , online supplemental figure S6D). In the VHL wild-type JAVELIN Renal 101 cohort, no significant difference in PFS was observed between the avelumab+axitinib arm and the sunitinib arm in the high OXPPOS group ( $p=0.15$ , online supplemental figure S6E), but PFS of the avelumab+axitinib arm was significantly better than that of the sunitinib arm in the low OXPPOS group ( $p=0.0087$ , online supplemental figure S6F).

VHL protein levels are affected by single nucleotide polymorphisms and epigenetic alterations such as copy number variation and methylation. Such events occur frequently in ccRCC,<sup>35</sup> while VHL mutations ultimately inhibit oxidative metabolism at the post-transcriptional level by promoting the transcription of PDK1, NDUFA4L2, and other genes.

Therefore, we used the data of PDK1 and NDUFA4L2 RNA expression to represent the VHL silencing status. Both genes were significantly highly expressed in VHL mutant cases (both  $p<0.001$ , online supplemental figure S5C,D). The expression levels of these genes were significantly higher in cluster 1 than in the other clusters (both  $p<0.001$ , online supplemental figure S5E, F). Thus, PDK1 and NDUFA4L2 are believed to better represent the VHL silencing state.

Based on the median expression of PDK1 and NDUFA4L2, patients were divided into high and low-expression groups. In the JAVELIN Renal 101 cohort with low expression of both genes, no significant difference in PFS was observed between the avelumab+axitinib arm and the sunitinib arm in the high OXPPOS group ( $p=0.54$ , online supplemental figure S7A), whereas the PFS of the avelumab+axitinib arm was significantly more favorable than that of the sunitinib arm in the low OXPPOS group ( $p=0.0087$ , online supplemental figure S7B). In clusters 2, 3, and 4 with low expression of both genes, no significant difference in PFS was observed between the avelumab+axitinib arm and the sunitinib arm in the high OXPPOS group ( $p=0.79$ , online supplemental figure S7C). However, in the low OXPPOS group, the PFS of the avelumab+axitinib arm was significantly better than that of the sunitinib arm ( $p=0.0023$ , online supplemental figure S7D). This result further demonstrates that the VHL status is a crucial factor interfering with the ability of OXPPOS to predict ICI efficacy.

### The predictive effect of OXPPOS was validated using the Tongji cohort

The clinicopathological data of 19 patients with TKI-resistant mRCC who were treated with anti-PD-1 combined with axitinib at Tongji Hospital were collected. The objective response rate (ORR) during treatment was evaluated through an imaging examination. During the follow-up period of 30–483 days, eight patients had disease progression, six patients exhibited SD, five patients had a PR, and no patient presented a CR. The ORR was 25%.

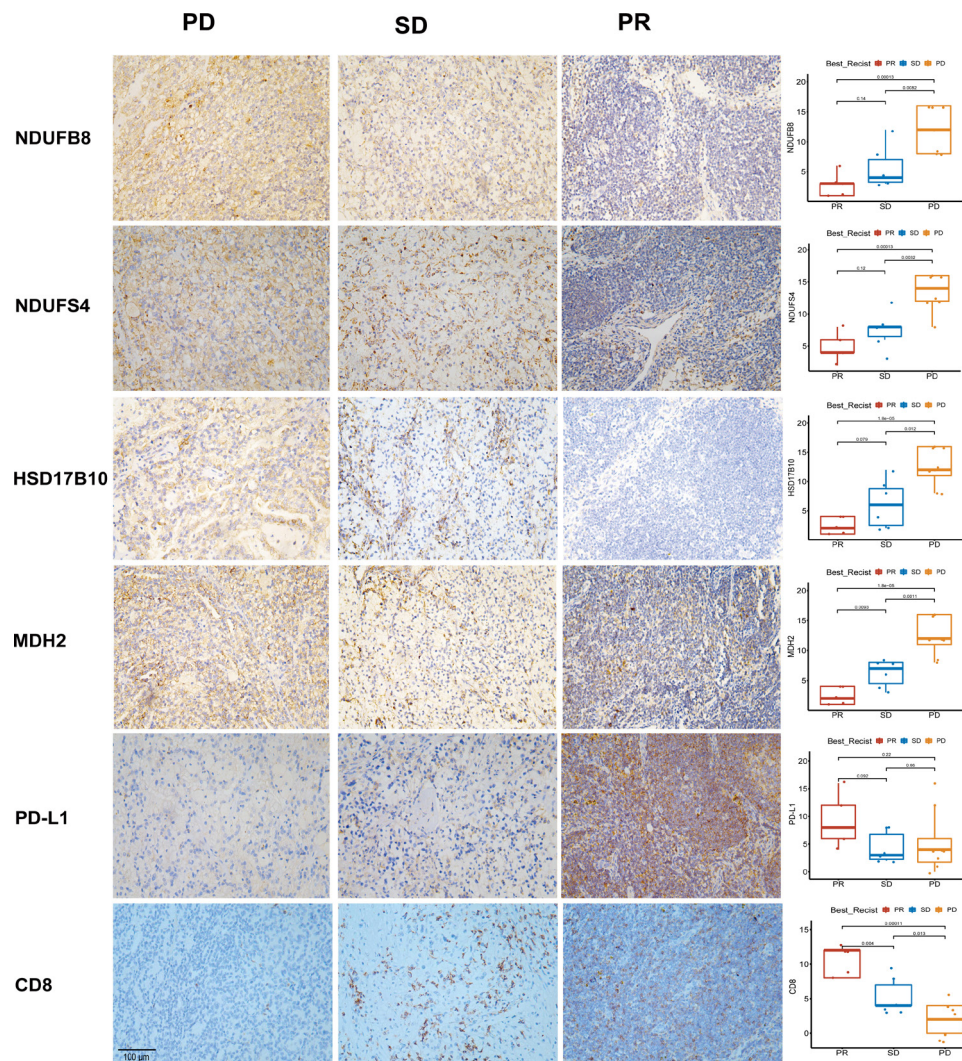


**Figure 3** Expression of OXPPOS-related protein in different objective-responses groups of Tongji cases. A significant difference was noted in the objective response rate between the high and low expression cases of OXPPOS-related proteins, and the expression was negatively correlated with CD8 and PD-L1 (magnification: 10×20). OXPPOS, oxidative phosphorylation; PD, progressive disease; PD-L1, programmed death ligand 1; PR, partial response; SD, stable disease.

IHC was performed using surgical or biopsy samples of these patients before initiating ICI treatment to evaluate the expression of OXPPOS-related proteins (including NDUFS4, NDUFB8, MDH2, and HSD17B10), CD8A, and PD-L1. A strong correlation was observed between OXPPOS-related proteins, and the expression of these proteins increased sequentially in PR, SD, and PD cases (figure 3). When NDUFB8 was considered as an example, PFS was significantly worse in the OXPPOS-related protein high expression group (log-rank test,  $p=0.0033$ , figure 4A), and the proportion of PR patients in this group was significantly reduced (Fisher's exact test,  $p=0.005$ , figure 4B). The PFS was better in the PD-L1 high expression group than in the low expression group, but the difference was not significant ( $p=0.12$ , figure 4C). No significant difference in the ORR was observed between the PD-L1 high and low expression groups (Fisher's exact test,  $p=0.593$ , figure 4D). The PFS was significantly better in the CD8 high expression group

than that in the low expression group (log-rank test,  $p=0.0023$ , figure 4E). The proportion of PR patients was significantly higher in the CD8 high expression group than in the low expression group (Fisher's exact test,  $p=0.005$ , figure 4F).

Cellular glucose metabolism mainly occurs through glycolysis or oxidative phosphorylation. In most cases, tumor cells favor glycolysis and the OXPPOS level decreases accordingly. Therefore, using the maximum standardized uptake value (SUVmax) of fluorodeoxyglucose-positron emission tomography/computed tomography (FDG-PET/CT), we indirectly evaluated the tumor OXPPOS level. In total, 15 patients were collected and FDG-PET/CT was performed 21 times. The procedure was performed 10 times before and 11 times after ICI treatment. All patients had 53 evaluable lesions after excluding repetitions, and 44 lesions could be evaluated continuously during treatment. Among these 44 lesions, maximum diameter decreased in 12

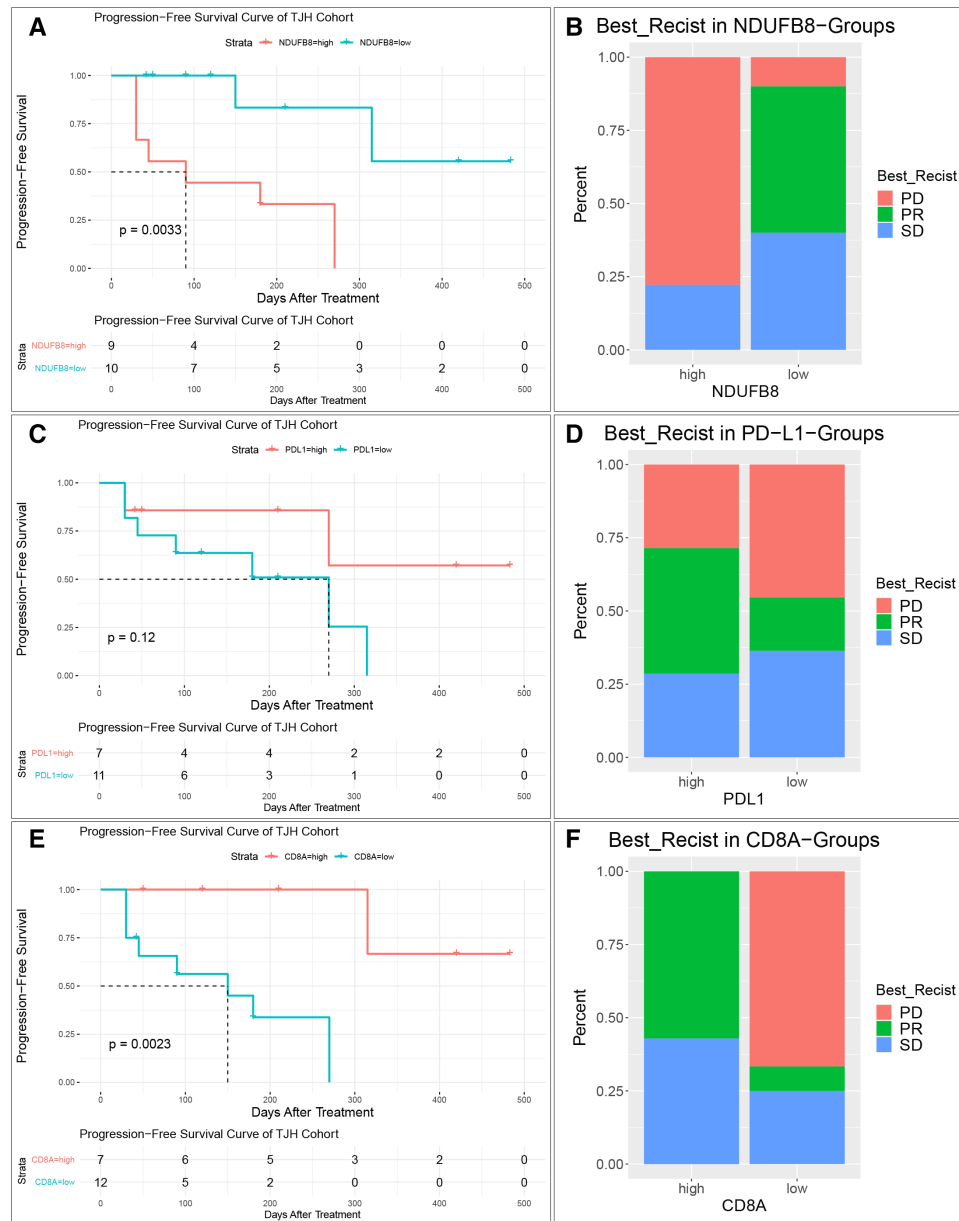


**Figure 4** Prediction of objective response rate and PFS by immunohistochemistry grouping of Tongji cases. (A) PFS was significantly worse in the group with a high expression of OXPHOS-related proteins, for example, NDUFB8 ( $p=0.0033$ ). (B) The proportion of PR patients in the NDUFB8 high-expression group was significantly reduced ( $p=0.005$ , Fisher's exact test). (C) The PFS of the PD-L1 high-expression group was better than that of the low-expression group, although the difference was insignificant ( $p=0.12$ ). (D) No significant difference was noted in the objective response rate between the PD-L1 high and low expression groups ( $p=0.593$ ). (E) The PFS of the CD8 high-expression group was significantly better than that of the low-expression group ( $p=0.0023$ ). (F) The proportion of PR patients in the CD8 high-expression group was significantly higher than that in the low-expression group ( $p=0.005$ ). OXPHOS, oxidative phosphorylation; PD, progressive disease; PD-L1, programmed death ligand 1; PFS, progression-free survival; PR, partial response; SD, stable disease.

lesions, increased in 16 lesions, and remained unchanged in another 16 lesions.

An evaluation of the SUVmax of the primary tumor FDG-PET/CT and IHC of the corresponding primary tumor tissue sections before immune checkpoint blockade (ICB) treatment revealed that expression of OXPHOS-related proteins was lower in tumors with higher SUVmax values (online supplemental figure S8).

The SUVmax of the primary tumor was higher than that of metastatic lesions ( $p<0.001$ ) and slightly higher than

that of the tumor thrombus, but not significant ( $p=0.057$ ). The SUVmax of the metastatic tumor was lower than that of the tumor thrombus ( $p=0.036$ , online supplemental figure S9A). The SUVmax of metastatic lesions significantly reduced after ICI treatment ( $p=0.016$ ). However, no significant change was observed in the SUVmax of the primary tumor ( $p=0.86$ ) and tumor thrombus ( $p=0.80$ ) before and after ICI treatment (online supplemental figure S9B).

Lesions with a reduced maximum diameter had a greater baseline SUVmax than those with enlarged and

unchanged maximum diameters (online supplemental figure S9C). This phenomenon was more obvious in metastatic lesions and tumor thrombi (both  $p < 0.001$ , online supplemental figure S9D). A scatter plot of the maximum diameter and SUVmax of the lesion revealed that SUVmax was positively correlated with the tumor's maximum diameter ( $R = 0.64$ ,  $p < 0.001$ ). The maximum diameter and SUVmax of the primary tumor were generally larger than those of the tumor thrombus and metastatic lesions (online supplemental figure S9E). In addition, ICI treatment mostly shrunk lesions with a smaller diameter and higher SUVmax (online supplemental figure S9F).

Although the glucose metabolism characteristics of tumors are related to their characteristics, they are not static. These glucose metabolism characteristics of tumor cells may vary in different environments or when exposed to specific treatments. This flexible mechanism facilitates tumor survival and progression.<sup>36–39</sup> We therefore sought to analyze the metabolic shift strategy of tumor cells in RCC.

In the CheckMate series, NDUFA4L2 RNA expression levels were significantly lower in the metastatic lesions than in the primary lesions (online supplemental figure S10A). On analyzing the TCGA-KIRP and TCGA-kidney chromophobe RCC (KICH) cohorts, we found that NDUFA4L2 expression was upregulated as tumor diameters increased (T1a to T2b) (online supplemental figure S10B,C). This indicated that as the tumor diameters increased, the OXPHOS level was gradually downregulated, and tumor cells re-biased to OXPHOS after hypoxia relief during metastasis and were possibly regulated by HIF-1 $\alpha$ .

The results of the analysis of Tongji's clinical data indicated that tumor cells in larger tumors (or primary tumors) can survive immunotherapy even in the absence of high OXPHOS levels. By contrast, in smaller tumors (or metastases), OXPHOS plays a key role in tumor cell resistance to ICI therapy.

To verify this conjecture, we compared the PFS of the high and low OXPHOS groups in the cases where the tissues collected from the CheckMate series were metastatic lesions. The PFS of the high OXPHOS group was significantly worse ( $p = 0.0044$ , online supplemental figure S10D). However, in the cases where the obtained tissue was a primary tumor, no significant difference in PFS was observed between the high and low OXPHOS groups ( $p = 0.63$ , online supplemental figure S10E).

### Tumor cell OXPHOS inhibits T-cell function and leads to immunotherapy resistance

According to previous studies, oxidative metabolism can affect immunotherapy by affecting CD8+cells. Therefore, we compared the correlation between the proportion of CD8+cells and OXPHOS at different tumor depths in the JAVELIN Renal 101 cohort. The low OXPHOS group had more CD8+cells in total ( $p = 0.0039$ , online supplemental figure S11A). Moreover, the closer to the tumor center, the more obvious the correlation between OXPHOS and

the cell proportion. On the surface of the tumor invasion margin, OXPHOS exhibited no significant correlation with the CD8+cells ( $p = 0.63$ , online supplemental figure S11B). By contrast, on the margin of tumor invasion, OXPHOS was negatively correlated with the CD8+cells ( $p = 0.05$ , online supplemental figure S11C). OXPHOS was also significantly negatively correlated with CD8+cells in the tumor center ( $p = 0.0015$ , online supplemental figure S11D).

To further identify the mechanism through which OXPHOS affects ICI therapy, we performed relevant pathway analysis by analyzing single-cell RNA-seq in tumor cells. The single-cell RNA-seq data of RCC were obtained from the study of Kevin *et al.*<sup>40</sup>

The single-cell classification was derived from the InferCNV analysis results published in the original article. The single sample gene set enrichment analysis (ssGSEA) score was obtained using a single tumor cell, and the gene sets used in the ssGSEA analysis were all from the HALL-MARK gene set. The OXPHOS score of the tumor cells was positively correlated with hypoxia ( $R = 0.74$ ,  $p < 0.001$ ), antigen presentation ( $R = 0.65$ ,  $p < 0.001$ ), reactive oxygen species (ROS,  $R = 0.91$ ,  $p < 0.001$ ), fatty acid metabolism ( $R = 0.88$ ,  $p < 0.001$ ), and other pathways (online supplemental figure S12), which were closely related to immunity.

To verify this finding in vivo and in vitro, we selected an OXPHOS-related molecule for knockdown. To avoid affecting other biological processes, we referred to previous studies and chose to knock down mitochondrial complex I. Mitochondrial complex I, also known as nicotinamide adenine dinucleotide (NAD/NADH) dehydrogenase, uses oxygen during OXPHOS and pumps protons into the mitochondrial inner membrane space for maintaining the mitochondrial membrane potential. It is also the main site for generating ROS. NDUF8 is a critical auxiliary subunit of mitochondrial complex I and is encoded by nuclear genes. This auxiliary subunit exhibited a stable and significant difference in our analysis. The loss of function of this auxiliary subunit can lead to the deficiency of mitochondrial complex I and OXPHOS downregulation<sup>41</sup>; therefore, NDUF8 was selected as the target.

Once Renca cells stably transfected with sh*Ndufb8* and shControl were obtained, real-time PCR was performed to determine the RNA knockdown efficiency. The knockdown efficiencies of sh*Ndufb8* 1 and sh*Ndufb8* 2 were 70% and 56%, respectively (figure 5A).

Then, the protein-level knockdown efficiency was evaluated through western blotting and analyzed through Imaging Lab V.6.0. The knockdown efficiencies of sh*Ndufb8* 1 and sh*Ndufb8* 2 were 61% and 22%, respectively (figure 5B). Because the sh*Ndufb8* 1 sequence stably knocked down *Ndufb8* expression in the Renca cells at RNA and protein levels, the sh*Ndufb8* 1 sequence was selected for subsequent experiments.

When sh*Ndufb8* Renca and shControl Renca grew to approximately 80% confluence, we sealed the culture

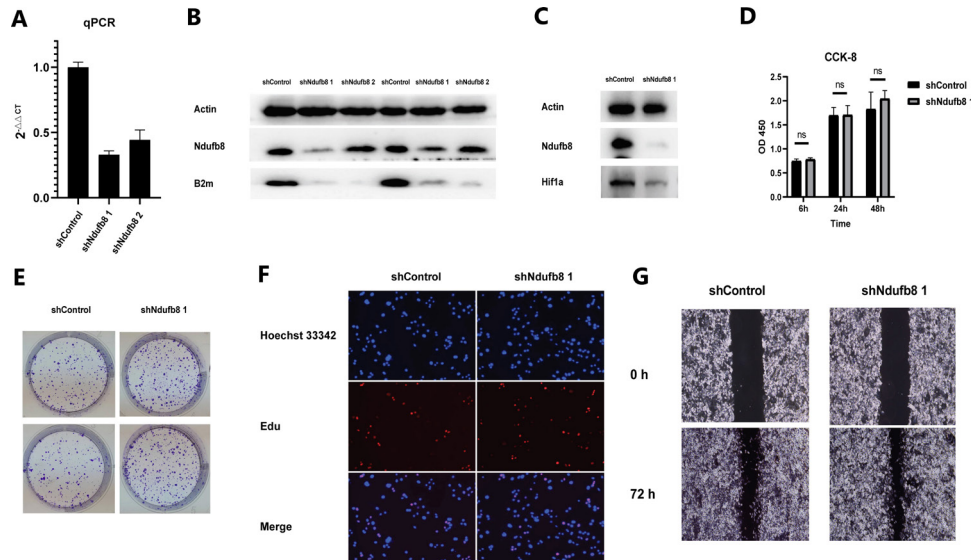


**Figure 5** Knockdown of NDUF8 does not affect the proliferation and migration of RENCA. (A) RNA-knockdown efficiency was tested by qPCR. The knockdown efficiency of sh*Ndufb8* 1 was 70%, while that of sh*Ndufb8* 2 was 56%. (B) Western blotting was performed to test the knockdown efficiency at the protein level. The knockdown efficiency of sh*Ndufb8* 1 was found to be 61%, while that of sh*Ndufb8* 2 was 22%. After *Ndufb8* was knocked down, the expression of B2m, a constituent molecule of antigen major histocompatibility complex I, was significantly downregulated. (C) The sh*Ndufb8* Renca cell line showed less HIF-1 $\alpha$  accumulation than shControl Renca after 8 hours of culture in a sealed environment. (D) The OD 450 after CCK-8 addition was measured at 24 hours and 48 hours, respectively, and there was no statistically significant difference in the proliferation of sh*Ndufb8* and shControl Renca cells at both times. (E) The colony-formation experiment performed to compare the proliferative ability of sh*Ndufb8* and shControl Renca cells revealed that the number of colonies formed by sh*Ndufb8* 1 Renca was slightly more than that of shControl Renca cells, although there was no statistically significant difference in the size of the colonies between the two cells. (F) Edu detects the proliferative ability. Edu and Hoechst 33342 mark the replicating DNA molecules and double-stranded DNA (nuclei), respectively, that is, mark proliferating cells and all cells. No significant difference was noted in the proportion of proliferating cells between sh*Ndufb8* 1 Renca and shControl Renca (magnification:  $\times 200$ ). (G) The cell scratch assay compared the migration ability of sh*Ndufb8* 1 Renca and shControl Renca cells, with no statistically significant difference in the 72 hours migration rate between the two cells. B2m, beta-2 microglobulin; HIF-1 $\alpha$ , hypoxia-inducible factor-1 $\alpha$ ; qPCR, quantitative PCR.

dishes with a sealing film, extracted the protein 8 hours later, and performed a western blot. We found that sh*Ndufb8* Renca cells had less HIF-1 $\alpha$  accumulation than the shControl Renca cells (figure 5C). In vitro cell function experiments were conducted before in vivo experiments to rule out the direct impact of OXPHOS on tumor cell proliferation and migration. The results proved that the OXPHOS level in tumor cells affects the TME, which in turn affects tumor growth in the mice.

The CCK-8 experiment revealed that after *Ndufb8* knockdown, no significant change in Renca cell proliferation was observed at 24 and 48 hours (figure 5D). Colony formation experiments proved that the proliferative ability of the sh*Ndufb8* Renca cells was not weakened compared with that of the shControl Renca cells (figure 5E).

In the Edu examination, Edu and Hoechst 33342 marked replicating DNA molecules and double-stranded DNA (nucleus), that is, they indicated the proliferating cells and all cells, respectively. No statistically significant difference was noted in the proportion of proliferating cells between the two cell types (figure 5F). The migration ability also exhibited no statistically significant difference between the sh*Ndufb8* Renca and shControl

Renca cells in the cell wound healing test (figure 5G). Therefore, knockdown of mitochondrial complex I did not affect the proliferation and migration of Renca cells in vitro.

In the in vivo experiment, the tumor growth rate of the same type of cells in the control group (IgG treatment group) was relatively similar, whereas that in the anti-PD-L1 treatment group varied. The anti-PD-L1 treatment failed to slow down the growth of some tumors, and the proportion of non-responsive tumors was lower in the sh*Ndufb8* group than in the shControl group (figure 6A–D). Additionally, in general, the growth rate of the sh*Ndufb8* Renca-generated tumors in the control group was significantly slower than that of the shControl Renca-generated tumors ( $p < 0.001$ ). The growth of the shControl+anti-PD-L1 group was slower than that of the shControl+IgG group ( $p < 0.001$ ). The growth of the sh*Ndufb8* Renca-generated tumors was significantly slower than that of the shControl Renca-generated tumors in the treatment group ( $p < 0.05$ ). The growth of the sh*Ndufb8* Renca-generated tumors in the treatment group was also significantly slower than that of the sh*Ndufb8* Renca-generated tumors in the control group ( $p < 0.001$ , figure 6E).

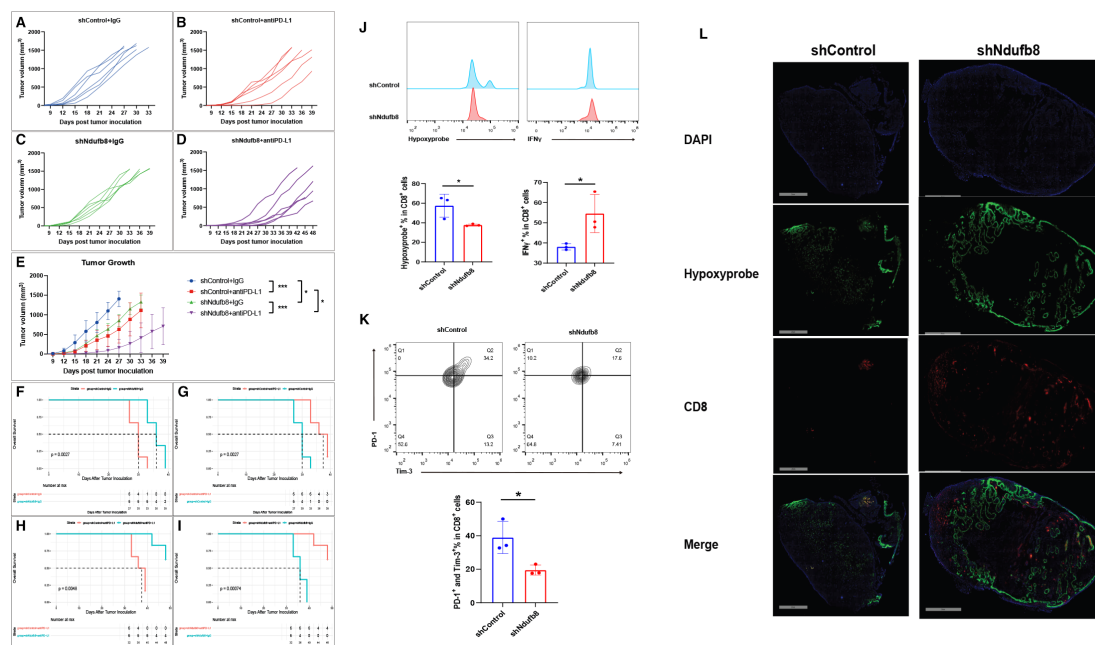


**Figure 6** *Ndufb8* knocking down increases the efficacy of immune checkpoint inhibitor in renal cell carcinoma in vivo. Tumor growth curves of the four groups of mice (A–D). (E) A comprehensive graph of tumor growth curve revealed that the growth rate of *shNdufb8*+IgG group was significantly slower than that of *shControl*+IgG ( $p < 0.001$ ), that of the *shControl*+anti-PD-L1 group was significantly slower than that of the *shControl*+IgG group ( $p < 0.001$ ), while that of the *shNdufb8*+anti-PD-L1 group was significantly slower than that of the *shControl*+anti-PD-L1 group ( $p < 0.05$ ). The growth velocity of the *shNdufb8*+anti-PD-L1 group was significantly slower than that of the *shNdufb8*+IgG group ( $p < 0.001$ ). Two-way analysis of variance tests were performed using GraphPad Prism V.9.0.0. (F) The survival of the mice in the *shNdufb8*+IgG group was significantly better than that in the *shControl*+IgG group ( $p = 0.0027$ ). (G) The survival of the mice in the *shControl*+anti-PD-L1 group was significantly better than that in the *shControl*+IgG group ( $p = 0.0027$ ). (H) The survival of mice in the *shNdufb8*+anti-PD-L1 group was significantly better than that in the *shControl*+anti-PD-L1 group ( $p = 0.0048$ ). (I) The survival of mice in the *shNdufb8*+anti-PD-L1 group was significantly better than that in the *shNdufb8*+IgG group ( $p < 0.001$ ). (J) The proportion of positive hypoxyprobe in the *shNdufb8* group was significantly lower than that in the *shControl* group ( $p < 0.05$ ), while the proportion of tumor-infiltrating CD8<sup>+</sup> T cells positive for IFN- $\gamma$  was significantly higher ( $p < 0.05$ ). (K) The proportion of PD-1<sup>+</sup> and TIM-3<sup>+</sup> positive tumor-infiltrating CD8<sup>+</sup> T cells in the *shNdufb8* group was significantly lower than that in the *shControl* group ( $p < 0.05$ ). (L) Immunofluorescence revealed that tumor-infiltrating CD8<sup>+</sup> T lymphocytes (red fluorescence) in the *shNdufb8* group were significantly more than those in the *shControl* group. The infiltrated CD8<sup>+</sup> T cells (red fluorescence) in the hypoxic area (green fluorescence) in the *shNdufb8* group were significantly lower than those in the non-hypoxic area. \* $p < 0.05$ , \*\* $p < 0.01$ . DAPI, 4',6-diamidino-2-phenylindole; IFN, interferon; PD-L1, PD-1, programmed death protein 1; pPD-L1, programmed death ligand 1; T-cell immunoglobulin domain and mucin domain 3.

During the observation period of up to 48 days, all mice in the *shControl*+IgG and *shNdufb8*+IgG groups died because of excessive tumor volume. Four mice in the *shControl*+anti-PD-L1 group died due to excessive tumor volume, and one mouse died due to tumor-induced poor nutritional status. Four mice in the *shControl*+anti-PD-L1 group died because of excessive tumor volume, and one mouse died due to tumor-induced poor nutritional status. Two mice in the *shNdufb8*+anti-PD-L1 group died because of excessive tumor volume.

Survival analysis revealed that the survival of mice in the *shNdufb8*+IgG group was significantly better than that in the *shControl*+IgG group ( $p = 0.0027$ , **figure 6F**). *Ndufb8* knockdown cannot slow down the Renca cell proliferation rate in vitro, but can slow down tumor growth in vivo. This suggests that the effect of *Ndufb8* knockdown on tumor growth is related to the TME. The survival of mice was significantly favorable in the *shControl*+anti-PD-L1 group than in the *shControl*+IgG group ( $p = 0.0027$ , **figure 6G**),

indicating that anti-PD-L1 had a certain suppressive effect on Renca-derived tumors. The survival of mice was significantly better in the *shNdufb8*+anti-PD-L1 group than in the *shControl*+anti-PD-L1 group ( $p = 0.0048$ , **figure 6H**). *Ndufb8* knockdown combined with anti-PD-L1 treatment significantly improved ICI efficacy. The survival of mice was significantly better in the *shNdufb8*+anti-PD-L1 group than in the *shNdufb8*+IgG group ( $p < 0.001$ , **figure 6I**), which suggested that *shNdufb8* Renca-derived tumors are more sensitive to anti-PD-L1 treatment.

Flow cytometry was performed using tumor-infiltrating lymphocytes in the knockdown and control groups. Because tumor cells can generate a hypoxic TME through OXPHOS, a hypoxyprobe stain was used in flow cytometry and immunofluorescence. The percentage of hypoxyprobe-positive CD8<sup>+</sup> T cells in tumor-infiltrating lymphocytes (TILs) from the *shNdufb8* group was significantly reduced ( $p < 0.05$ , **figure 6J**), whereas the percentage of IFN- $\gamma$ <sup>+</sup> CD8<sup>+</sup> T cells was significantly increased ( $p < 0.05$ ,

figure 6J). *Ndufb8* knockdown is suggested to significantly reduce the exposure of tumor-infiltrating CD8<sup>+</sup> T cells to hypoxia and enhance their ability to kill tumor cells.

PD-1 and TIM-3 were detected on the surface of tumor-infiltrating CD8<sup>+</sup> T cells in the sh*Ndufb8* and shControl groups. The proportion of CD8<sup>+</sup> T cells positive for the expression of both PD-1 and TIM-3 was significantly reduced in the sh*Ndufb8* group ( $p < 0.05$ , figure 6K). *Ndufb8* knockdown possibly alleviates the degree of exhaustion of tumor-infiltrating CD8<sup>+</sup> T cells.

Immunofluorescence experiments revealed that tumor-infiltrating T lymphocytes (red fluorescence) were significantly more in the sh*Ndufb8* group than in the shControl group. In the sh*Ndufb8* group, the proportion of CD8<sup>+</sup> T cells (red fluorescence) was significantly lower in the hypoxic area (green fluorescence) than in the non-hypoxic area (figure 6L). Altogether, the aforementioned data confirm that OXPHOS inhibits the T-cell function by creating a hypoxic TME, thereby leading to resistance to anti-PD-L1 therapy.

## DISCUSSION

The impact of OXPHOS on ICI resistance has rarely been explored. A limited number of studies have supported that OXPHOS leads to immunotherapy resistance focused on the mechanism by which tumor cells produce hypoxic TME through OXPHOS, which then inhibits the T-cell function. In 2017, Scharping *et al* found that OXPHOS of tumor cells (melanoma B16 and colon cancer MC38 cell lines) can lead to the generation of a hypoxic TME, thereby reducing the proliferative and tumor-killing abilities of T cells. The mitochondrial complex I inhibitor metformin significantly improved the response rate of anti-PD-1 therapy. When treated with a combination of metformin and anti-PD-1 antibody, all MC38 tumor-bearing mice exhibited tumor regression, 88% of the tumors exhibited complete regression, 80% regression, and 70% complete regression was noted in B16 tumor-bearing mice.<sup>42</sup> A consistent pattern was noted in RCC, and the interference of VHL mutations possibly caused this pattern to be ignored by previous researchers.

In a small retrospective study comparing metformin+ICI versus ICI alone against metastatic malignant melanoma, the ORR, disease control rate, OS, and PFS were superior in the metformin+ICI-treated group. However, the differences were not statistically significant in the multivariate analysis, considering that the average number of new metastatic sites that emerged during treatment was significantly higher in the combination group.<sup>43</sup> This finding is consistent with the results of our study that OXPHOS is crucial for resistance to ICI therapy in small/metastatic lesions but less so in large/primary tumors.

According to Najjar *et al*, malignant melanoma cells inhibit the T-cell function by creating a hypoxic TME through OXPHOS, and knockdown of the mitochondrial complex I subunit *Ndufs4* in ICI-resistant melanoma cell lines causes tumors generated by this cell line to respond

to ICI. The key to this reduction in resistance is that the degree of hypoxia is eliminated, which is consistent with the results of our study.<sup>22</sup>

However, Harel *et al* used proteomics to compare samples of responders and non-responders who received immunotherapy (TIL adoptive or anti-PD-1) for malignant melanomas. They found that the expression of OXPHOS-related proteins in tumor tissues was significantly higher in the responders than in the non-responders. Once the OXPHOS-related gene *Acat1* was knocked out, the melanoma cell line grew faster than the control group in vivo and in vitro. Co-culturing of the melanoma cell line with T cells weakened the ability of T cells to kill tumor cells. This is perhaps not contradictory to the results of our study, because Harel *et al* did not directly knockdown mitochondrial complexes and did not apply immunotherapy in vivo. Additionally, in this study, after OXPHOS-related genes were knocked down, the expression of antigen presentation-related proteins was downregulated and the melanoma cells became insensitive to T-cell killing, which is in agreement with the results of our study that OXPHOS positively correlates with antigen presentation and B2m is downregulated after *Ndufb8* knockdown.<sup>44</sup>

Valle *et al* induced a pancreatic ductal adenocarcinoma cell line that prefers OXPHOS through a galactose medium. They found that the characteristics of tumor stem cells were significantly upregulated compared with the control cell line. Moreover, the tumor stem cells were resistant to multiple chemotherapeutic drugs and expressed various immune evasion-related molecules.<sup>45</sup> In non-small cell lung cancer cell lines, the basal and reserve OXPHOS levels were higher in anti-PD-1 therapy-resistant cell lines than in the sensitive cell lines. Radiation therapy could reverse the resistance of the ICI-resistant cell lines while increasing its OXPHOS. The OXPHOS inhibitor IACS-010759 combined with radiotherapy could reverse the resistance of ICI-resistant tumors to a greater extent. However, in the treatment of ICI-sensitive tumors, IACS-010759 failed to further reduce tumor growth when combined with radiotherapy.<sup>46</sup>

Currently, some OXPHOS inhibitors, such as IACS-010759, devimistat, and IM156, are used in phase I and II clinical trials.<sup>19 47 48</sup> Moreover, metformin, a safe drug approved for diabetes, inhibits OXPHOS.<sup>43</sup> All the aforementioned drugs inhibit OXPHOS by inhibiting mitochondrial complex I.

In 2021, using an in vitro co-culture system, Scharping *et al* systematically assessed the effects of hypoxia and antigen stimulation on T-cell exhaustion. They found that continuous hypoxia and antigen stimulation significantly inhibited T-cell expansion and increased the proportion of terminally exhausted T cells. The inhibitory effect of continuous hypoxia and antigen stimulation on the T cells was significantly stronger than that on the T cells cultured under hypoxic conditions without continuous antigen stimulation or under normoxic conditions without continuous antigen stimulation.<sup>9</sup> Consistently, in this study, higher OXPHOS levels meant higher hypoxia



and antigen presentation levels. These two factors were the initiators of the terminal exhaustion of T cells in Scharping *et al's* study. Furthermore, Scharping *et al* found that once the T cells were exposed to continuous hypoxia and antigenic stimulation for a certain time and the proportion of terminally exhausted T cells increased, the exhausted state of T cells could not be rescued even if they were returned to normoxic conditions. According to our findings, early metastatic tumors (smaller in size) use higher OXPHOS levels, and as the size of these tumors increases, they tend to use glycolytic metabolism. Therefore, in larger tumors, even if OXPHOS levels are lower, the infiltrating T cells are also mainly exhausted. Therefore, OXPHOS levels are critical for ICI resistance in small-volume tumors, such as metastatic lesions, but they are not sufficiently significant in larger-volume tumors such as primary lesions.

Our study still has some deficiencies. For example, we only described the OXPHOS phenomenon that leads to ICI resistance but failed to further design experiments to clarify the underlying mechanism. The sample size of clinical cases was small, and the bias of retrospective studies existed. OXPHOS levels were assessed through FDG-PET/CT, which is an indirect evidence. More in-depth experiments are required to understand the underlying mechanism, and higher quality evidence support is warranted in clinical research.

**Correction notice** This article has been corrected since it was first published. Figure 5 contained incorrect images and these have now been replaced.

**Acknowledgements** The authors would like to thank the patients who agreed to participate in this retrospective study as well as Jihong Liu, President of Tongji Hospital, and Shaogang Wang, Director of the Department of Urology, who made this study possible.

**Contributors** JT is guarantor and responsible for the overall content, and contributed to the design of the study, data collection and analysis, in vivo and in vitro experiments, manuscript writing and modification. JL contributed to the manuscript modification. XZ contributed to data interpretation, providing cases, discussing experimental arrangements and literature sharing. CK, YW and YZ contributed to data interpretation and literature sharing. ZL and LL assisted with the in vitro and in vivo experiments. ZH and CY contributed by providing cases, manuscript modification, data interpretation, and discussion on experimental arrangements.

**Funding** This work was supported by the National Natural Science Foundation of China (No. 81702989).

**Competing interests** No, there are no competing interests.

**Patient consent for publication** Consent obtained directly from patient(s).

**Ethics approval** This study involves human participants and was approved by Clinical Trial Ethics Committee of Tongji Hospital; TJ-IRB-20230331; Animal Care and Use Committee of Tongji Hospital (TJH-201910012). Participants gave informed consent to participate in the study before taking part.

**Provenance and peer review** Not commissioned; externally peer reviewed.

**Data availability statement** Data are available in a public, open access repository. Data from Checkmate (1), NCT01358721 (2) and Javelin Renal 101 (3) can be obtained from the original articles. Survival and response data from Tongji Hospital can be obtained by requesting the author. References: (1) Braun, DA, *et al*. Interplay of somatic alterations and immune infiltration modulates response to PD-1 blockade in advanced clear cell renal cell carcinoma. *NAT MED* 26, 909–918 (2020). (2) Ross-Macdonald, P, *et al*. Molecular correlates of response to nivolumab at baseline and on treatment in patients with RCC., Vol. 9(2021). (3) Motzer, RJ, *et al*. Avelumab plus axitinib versus sunitinib in advanced renal cell carcinoma: biomarker analysis of the phase 3 JAVELIN Renal 101 trial. *NAT MED* 26, 1733–1741 (2020).

**Supplemental material** This content has been supplied by the author(s). It has not been vetted by BMJ Publishing Group Limited (BMJ) and may not have been peer-reviewed. Any opinions or recommendations discussed are solely those of the author(s) and are not endorsed by BMJ. BMJ disclaims all liability and responsibility arising from any reliance placed on the content. Where the content includes any translated material, BMJ does not warrant the accuracy and reliability of the translations (including but not limited to local regulations, clinical guidelines, terminology, drug names and drug dosages), and is not responsible for any error and/or omissions arising from translation and adaptation or otherwise.

**Open access** This is an open access article distributed in accordance with the Creative Commons Attribution Non Commercial (CC BY-NC 4.0) license, which permits others to distribute, remix, adapt, build upon this work non-commercially, and license their derivative works on different terms, provided the original work is properly cited, appropriate credit is given, any changes made indicated, and the use is non-commercial. See <http://creativecommons.org/licenses/by-nc/4.0/>.

#### ORCID id

Chunguang Yang <http://orcid.org/0000-0002-3882-4940>

#### REFERENCES

- Albiges L, Tannir NM, Burotto M, *et al*. First-line nivolumab plus ipilimumab versus sunitinib in patients without nephrectomy and with an evaluable primary renal tumor in the checkmate 214 trial. *EUR UROL* 2022;81:266–71.
- Powles T, Plimack ER, Soulières D, *et al*. Pembrolizumab plus axitinib versus sunitinib monotherapy as first-line treatment of advanced renal cell carcinoma (KEYNOTE-426): extended follow-up from a randomised, open-label, phase 3 trial. *The Lancet Oncology* 2020;21:1563–73.
- Choueiri TK, Powles T, Burotto M, *et al*. Nivolumab plus cabozantinib versus sunitinib for advanced renal-cell carcinoma. *N Engl J Med* 2021;384:829–41.
- Motzer RJ, Penkov K, Haanen J, *et al*. Avelumab plus axitinib versus sunitinib for advanced renal-cell carcinoma. *N Engl J Med* 2019;380:1103–15.
- Ljungberg B, Albiges L, Abu-Ghanem Y, *et al*. European association of urology guidelines on renal cell carcinoma: the 2022 update. *Eur Urol* 2022;82:399–410.
- Bader JE, Voss K, Rathmell JC. Targeting metabolism to improve the tumor microenvironment for cancer immunotherapy. *MOL CELL* 2020;78:1019–33.
- Kubli SP, Berger T, Araujo DV, *et al*. Beyond immune checkpoint blockade: emerging immunological strategies. *Nat Rev Drug Discov* 2021;20:899–919.
- Cho SH, Raybuck AL, Stengel K, *et al*. Germinal centre hypoxia and regulation of antibody qualities by a hypoxia response system. *NATURE* 2016;537:234–8.
- Scharping NE, Rivadeneira DB, Menk AV, *et al*. Mitochondrial stress induced by continuous stimulation under hypoxia rapidly drives T cell exhaustion. *NAT IMMUNOL* 2021;22:205–15.
- Terry S, Engelsens AST, Buart S, *et al*. Hypoxia-driven intratumor heterogeneity and immune evasion. *CANCER LETT* 2020;492:1–10.
- Warburg O, Wind F, Negelein E. THE METABOLISM OF TUMORS IN THE BODY. *J Gen Physiol* 1927;8:519–30.
- Lunt SY, Vander Heiden MG. Aerobic glycolysis: meeting the metabolic requirements of cell proliferation. *ANNU REV CELL DEV Biol* 2011;27:441–64.
- Koppenol WH, Bounds PL, Dang CV. Otto Warburg's contributions to current concepts of cancer metabolism. *Nat Rev Cancer* 2011;11:325–37.
- Birsoy K, Wang T, Chen WW, *et al*. An essential role of the mitochondrial electron transport chain in cell proliferation is to enable aspartate synthesis. *CELL* 2015;162:540–51.
- Ju YS, Alexandrov LB, Gerstung M, *et al*. Origins and functional consequences of somatic mitochondrial DNA mutations in human cancer. *ELIFE* 2014;3:e02935.
- Weinberg F, Hamanaka R, Wheaton WW, *et al*. Mitochondrial metabolism and ROS generation are essential for Kras-mediated tumorigenicity. *Proc Natl Acad Sci USA* 2010;107:8788–93.
- Sullivan LB, Gui DY, Hosios AM, *et al*. Supporting aspartate biosynthesis is an essential function of respiration in proliferating cells. *CELL* 2015;162:552–63.
- Zhou Y, Tozzi F, Chen J, *et al*. Intracellular ATP levels are a pivotal determinant of chemoresistance in colon cancer cells. *CANCER RES* 2012;72:304–14.

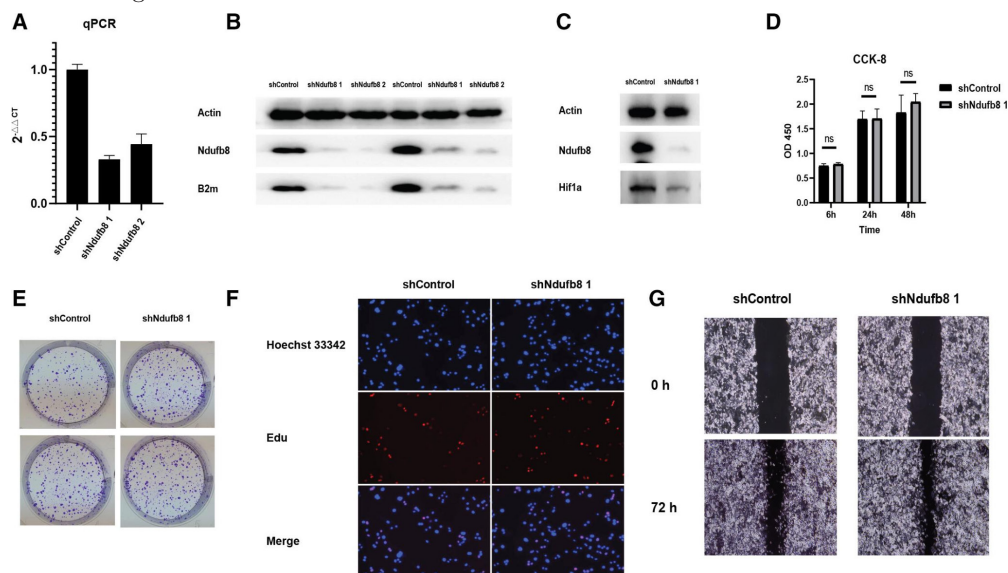
- 19 Molina JR, Sun Y, Protopopova M, *et al.* An inhibitor of oxidative phosphorylation exploits cancer vulnerability. *NAT MED* 2018;24:1036–46.
- 20 Hasim MS, Marotel M, Hodgins JJ, *et al.* When killers become thieves: trogocytosed PD-1 inhibits NK cells in cancer. *SCI ADV* 2022;8.
- 21 LeBleu VS, O'Connell JT, Gonzalez Herrera KN, *et al.* PGC-1 $\alpha$  mediates mitochondrial biogenesis and oxidative phosphorylation in cancer cells to promote metastasis. *NAT CELL BIOL* 2014;16:992–1003.
- 22 Najjar YG, Menk AV, Sander C, *et al.* Tumor cell oxidative metabolism as a barrier to PD-1 blockade immunotherapy in melanoma. *JCI Insight* 2019;4:e124989.
- 23 Miao D, Margolis CA, Gao W, *et al.* Genomic correlates of response to immune checkpoint therapies in clear cell renal cell carcinoma. *Science* 2018;359:801–6.
- 24 Braun DA, Hou Y, Bakouny Z, *et al.* Interplay of somatic alterations and immune infiltration modulates response to PD-1 blockade in advanced clear cell renal cell carcinoma. *NAT MED* 2020;26:909–18.
- 25 Motzer RJ, Robbins PB, Powles T, *et al.* Avelumab plus axitinib versus sunitinib in advanced renal cell carcinoma: biomarker analysis of the phase 3 JAVELIN Renal 101 trial. *NAT MED* 2020;26:1733–41.
- 26 Ross-Macdonald P, Walsh AM, Chasalow SD, *et al.* Molecular correlates of response to nivolumab at baseline and on treatment in patients with RCC. *J Immunother Cancer* 2021;9:e001506.
- 27 Schwartz LH, *et al.* RECIST 1.1-Update and clarification: from the RECIST committee. *European journal of cancer*. 1990;62:132–7.
- 28 Li H, Zhang Y, Li D, *et al.* Androgen receptor splice variant 7 predicts shorter response in patients with metastatic hormone-sensitive prostate cancer receiving androgen deprivation therapy. *EUR UROL* 2021;79:879–86.
- 29 Kim J, Tchernyshyov I, Semenza GL, *et al.* HIF-1-mediated expression of pyruvate dehydrogenase kinase: A metabolic switch required for cellular adaptation to hypoxia. *CELL Metabolism* 2006;3:177–85.
- 30 Li H-S, Zhou Y-N, Li L, *et al.* HIF-1 $\alpha$  protects against oxidative stress by directly targeting mitochondria. *REDOX BIOL* 2019;25:101109.
- 31 Maxwell PH, Wiesener MS, Chang GW, *et al.* The tumour suppressor protein VHL targets hypoxia-inducible factors for oxygen-dependent proteolysis. *NATURE* 1999;399:271–5.
- 32 Liu X, Xie P, Hao N, *et al.* HIF-1-regulated expression of calreticulin promotes breast tumorigenesis and progression through Wnt/ $\beta$ -catenin pathway activation. *Proc NATL ACAD SCI USA* 2021;118.
- 33 Tsao C-C, Baumann J, Huang S-F, *et al.* Pericyte hypoxia-inducible factor-1 (HIF-1) drives blood-brain barrier disruption and impacts acute ischemic stroke outcome. *ANGIOGENESIS* 2021;24:823–42.
- 34 You L, Wu W, Wang X, *et al.* The role of hypoxia-inducible factor 1 in tumor immune evasion. *MED RES REV* 2021;41:1622–43.
- 35 Shenoy N, Pagliaro L. Sequential pathogenesis of metastatic VHL mutant clear cell renal cell carcinoma: putting it together with a translational perspective. *Ann Oncol* 2016;27:1685–95.
- 36 DeBerardinis RJ, Chandel NS. Fundamentals of cancer metabolism. *SCI ADV* 2016;2:e1600200.
- 37 Cruz-Bermúdez A, Laza-Briviesca R, Vicente-Blanco RJ, *et al.* Cisplatin resistance involves a metabolic reprogramming through ROS and PGC-1 $\alpha$  in NSCLC which can be overcome by OXPHOS inhibition. *Free Radical Biology and Medicine* 2019;135:167–81.
- 38 Li T, Han J, Jia L, *et al.* PKM2 coordinates glycolysis with mitochondrial fusion and oxidative phosphorylation. *PROTEIN CELL* 2019;10:583–94.
- 39 Fernández-Vizarrá E, López-Calcerrada S, Sierra-Magro A, *et al.* Two independent respiratory chains adapt OXPHOS performance to glycolytic switch. *CELL METAB* 2022;34:1792–808.
- 40 Bi K, He MX, Bakouny Z, *et al.* Tumor and immune reprogramming during immunotherapy in advanced renal cell carcinoma. *CANCER CELL* 2021;39:649–61.
- 41 Piekutowska-Abramczuk D, Assouline Z, Mataković L, *et al.* NDUFB8 mutations cause mitochondrial complex I deficiency in individuals with leigh-like encephalomyopathy. *AM J HUM GENET* 2018;102:460–7.
- 42 Scharping NE, Menk AV, Whetstone RD, *et al.* Efficacy of PD-1 blockade is potentiated by metformin-induced reduction of tumor hypoxia. *CANCER IMMUNOL RES* 2017;5:9–16.
- 43 Afzal MZ, Mercado RR, Shirai K. Efficacy of metformin in combination with immune checkpoint inhibitors (anti-PD-1/anti-CTLA-4) in metastatic malignant melanoma. *J IMMUNOTHER CANCER* 2018;6:64.
- 44 Harel M, Ortenberg R, Varanasi SK, *et al.* Proteomics of melanoma response to immunotherapy reveals mitochondrial dependence. *CELL* 2019;179:236–50.
- 45 Valle S, Alcalá S, Martín-Hijano L, *et al.* Exploiting oxidative phosphorylation to promote the stem and immunoevasive properties of pancreatic cancer stem cells. *NAT COMMUN* 2020;11:5265.
- 46 Chen D, Barsoumian HB, Fischer G, *et al.* Combination treatment with radiotherapy and a novel oxidative phosphorylation inhibitor overcomes PD-1 resistance and enhances antitumor immunity. *J IMMUNOTHER CANCER* 2020;8:e000289.
- 47 Mohan A, Griffith KA, Wuchu F, *et al.* Devimistat in combination with gemcitabine and cisplatin in biliary tract cancer: preclinical evaluation and phase Ib multicenter clinical trial (BiIT-04). *Clin Cancer Res* 2023;29:2394–400.
- 48 Janku F, *et al.* First-in-human study of Im156, a novel potent Biguanide oxidative Phosphorylation (OXPHOS). In: *inhibitor, in patients with advanced solid tumors* 401001–1010. 2022:

## Correction: Targeting oxidative phosphorylation to increase the efficacy of immune-combination therapy in renal cell carcinoma

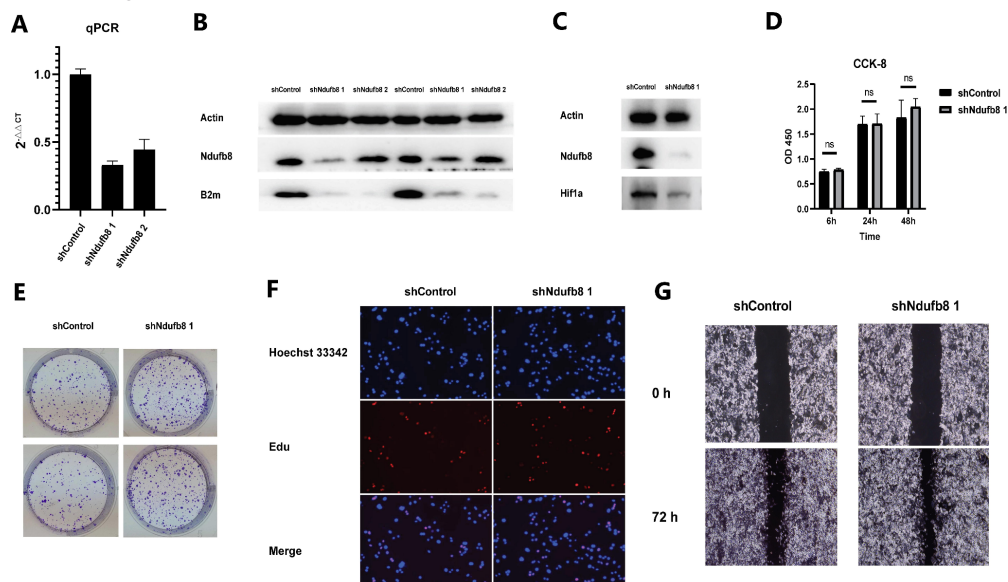
Tian J, Luo J, Zeng X, *et al.* Targeting oxidative phosphorylation to increase the efficacy of immune-combination therapy in renal cell carcinoma. *J Immunother Cancer* 2024;12:e008226. doi: 10.1136/jitc-2023-008226

This article has been corrected since it was first published. Figure 5 contained incorrect images due to a pasting error in the figure assembly process. All images have now been replaced with the correct versions.

Previous figure:



Correct figure:



**Open access** This is an open access article distributed in accordance with the Creative Commons Attribution Non Commercial (CC BY-NC 4.0) license, which permits others to distribute, remix, adapt, build upon this work non-commercially, and license their derivative works on different terms, provided the original work is properly cited, appropriate credit is given, any changes made indicated, and the use is non-commercial. See <http://creativecommons.org/licenses/by-nc/4.0/>.

© Author(s) (or their employer(s)) 2024. Re-use permitted under CC BY-NC. No commercial re-use. See rights and permissions. Published by BMJ.

*J Immunother Cancer* 2024;**12**:e008226corr1. doi:10.1136/jitc-2023-008226corr1

